Acta Cryst. (1977). B**33**, 3802–3813

Some Structures Topologically Related to Cubic Perovskite ($E2_1$), ReO_3 ($D0_9$) and Cu_3Au ($L1_2$)

BY M. O'KEEFFE

Chemistry Department, Arizona State University, Tempe, Arizona 85281, *USA*

AND B. G. HYDE*

*Gorlaeus Laboratories, Rijksuniversiteit, PB*75, *Leiden, The Netherlands*

(*Received* 5 *April* 1977; *accepted* 9 *June* 1977)

The following structure types are related to those in the title by regular patterns of concerted rotations of BX_6 octahedra about their $\bar{3}$ axes, the topology being unchanged: WAl_{12}, $Sc(OH)_3$, $NaMn_7O_{12}$, skutterudite, PdF_3, $LiNbO_3$, $NaSb(OH)_6$, Fe_3C, $BiCl_3$, YF_3, $GdFeO_3$, $UCrS_3$, *etc.* The cuboctahedral interstices in the parent structures are eventually transformed into icosahedra, rhombic prisms, octahedra, cubes, square antiprisms and/or trigonal prisms. Some consideration is also given to the tysonite (LaF_3) structure; to direct relations between the different derived structure types; and to some structures derived from $L1_2$ by rotations of octahedra about fourfold axes.

In an earlier paper (O'Keeffe & Hyde, 1976) we showed how the structures of a number of binary and ternary compounds could be derived from a parent structure or *aristotype* (Megaw, 1973) which was the filled $C9$ structure (the idealized, cubic cristobalite modification of SiO_2). This has stoichiometry ABX_2, and is characterized by a framework of BX_4 tetrahedra linked by their corners. Derived structures were obtained by rotating the tetrahedra about their $\bar{4}$ axes in a way which maintained a uniform B–X–B angle, and preserved the regularity of the tetrahedra. We now consider the effects of analogous rotations on an analogous array of corner-connected octahedra.

* Present address: School of Chemistry, University of Western Australia, Nedlands, WA 6009, Australia.

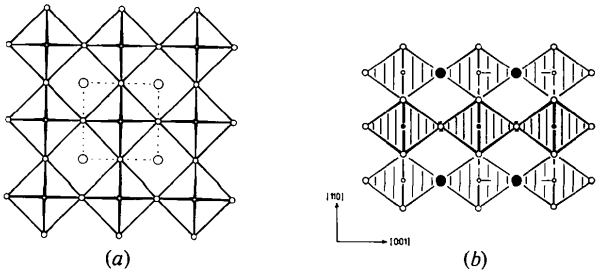

Fig. 1. The 'ideal', cubic perovskite structure, ABX_3, projected along (*a*) [001], (*b*) [1$\bar{1}$0]. In (*a*) the large circles are A atoms at $z = 0$, the medium circles are X atoms at $z = \frac{1}{2}$, and the very small circles are X atoms at $z = 0$ and B atoms at $z = \frac{1}{2}$. The BX_6 octahedra are outlined, and the broken line indicates the unit cell. In (*b*) the largest circles are A atoms at $\frac{1}{2}$ (open, partly obscured) and 0 (filled); medium circles are X atoms, some at 0, some at $\frac{1}{2}$; and the smallest circles are B atoms at $\frac{1}{2}$ (open) and 0 (filled). The BX_6 octahedra are emphasized.

The aristotype is the 'ideal', cubic perovskite structure, $E2_1$, Fig. 1. This has stoichiometry ABX_3, and is a filled **ReO_3** ($D0_9$) type: the A atoms are accommodated in cuboctahedral cavities in the framework of BX_6 octahedra. AX_3 has the structure of **$AuCu_3$** ($L1_2$), and A and B together form the **CsCl** ($B2$) structure.† The symmetry is cubic, space group $Pm3m$, with A in 1(*a*), B in 1(*b*), and X in 3(*c*). As in the earlier paper, we explore the ways in which the framework can collapse to produce denser structures. Discussion is limited to the simpler ways of doing this, and concentrated on those distortions which, as far as possible, maintain a uniform B–X–B angle. In the aristotype this bond angle is 180° which means, since the bonds are directed along ⟨100⟩, rotating the octahedra about axes that make equal angles with all ⟨100⟩ directions, *i.e.* about ⟨111⟩.

The problem of describing the distortions of the perovskite structure is, of course, not new. In particular, Glazer (1972) has considered all possible combinations of rotations about ⟨100⟩, subject to the constraint that the periodicity of the derived structure is not more than twice the unit-cell edge of the parent structure. In this paper, within the same constraint, we develop some of his results and consider, as well as 'perovskites', those other compounds that fall into this structural family. Glazer found 22 possibilities (not all of which are feasible if the octahedra are to remain regular). In the limit of small rotations four of these correspond to rotations about ⟨111⟩. In his notation

† Formulae in bold face represent structure types; those in ordinary fount represent chemical compounds. When no reference is given for a structure it may be found in one of the standard compilations, *e.g.* Schubert (1964).

Table 1. *Patterns of rotation axes of octahedra centred at the corners of the ideal perovskite unit cell*

The x axis is vertical, pointing down the page; the y axis is horizontal, pointing from left to right. First and second layer refers to octahedra with centres at $z = 0$ and $z = 1$.

	First layer		Second layer	
(i)	[111]	[$\bar{1}$11]	[$\bar{1}\bar{1}\bar{1}$]	[1$\bar{1}\bar{1}$]
	[111]	[$\bar{1}$11]	[$\bar{1}\bar{1}\bar{1}$]	[111]
(ii)	[111]	[$\bar{1}\bar{1}\bar{1}$]	[$\bar{1}\bar{1}\bar{1}$]	[111]
	[$\bar{1}\bar{1}\bar{1}$]	[111]	[111]	[$\bar{1}\bar{1}\bar{1}$]
(iii)	[111]	[$\bar{1}$1$\bar{1}$]	[$\bar{1}\bar{1}\bar{1}$]	[1$\bar{1}$1]
	[1$\bar{1}\bar{1}$]	[$\bar{1}$11]	[$\bar{1}$11]	[11$\bar{1}$]
(iv)	[111]	[$\bar{1}\bar{1}\bar{1}$]	[$\bar{1}\bar{1}\bar{1}$]	[111]
	[11$\bar{1}$]	[$\bar{1}$11]	[$\bar{1}$11]	[11$\bar{1}$]
(v)	[001]	[00$\bar{1}$]	[001]	[00$\bar{1}$]
	[00$\bar{1}$]	[001]	[001]	[001]
(vi)	[001]	[001]	[00$\bar{1}$]	[001]
	[00$\bar{1}$]	[001]	[001]	[00$\bar{1}$]

they are (i) $a^+a^+a^+$, (ii) $a^-a^-a^-$, (iii) $a^+a^+a^-$, (iv) $a^+a^-a^-$. As discussed below, only the first two correspond strictly to rotations about $\langle 111 \rangle$, and to uniform $B-X-B$ angles: for the last two the rotation axes have to undergo tilts with respect to each other if the octahedra are to remain regular; and there are, in these cases, two different $B-X-B$ angles.

The nature of the rotations can be understood by specifying the rotation axes of the eight octahedra with centres at the corners of the perovskite unit cell, *i.e.* for a 2 × 2 × 2 'supercell'. These are shown for the four systems (i) to (iv) in Table 1, adopting the convention that rotation is clockwise when viewed in the direction of the axis (so that, for example, [111] and [$\bar{1}\bar{1}\bar{1}$] represent rotations about the same axis, but in opposite senses). The size of the octahedra is maintained constant, the $B-X$ distance being d and the octahedron-edge length $\sqrt{2}d$.

Each of the rotation systems is now considered separately.

Sequence (i): structures with cubic, *Im*3 symmetry

The first system involves rotations about four different $\langle 111 \rangle$ directions, and produces a new structure $A'A''_3B_4X_{12}$ with unit-cell edges approximately doubled. The transformation matrix for the new unit cell is 200/020/002; and the structure can be expressed in terms of the rotation angle φ as follows.

Space group *Im*3 (No. 204); $a = d(8 \cos \varphi + 4)/3$.
Unit-cell volume $V(\varphi) = V(0)(2 \cos \varphi + 1)^3/27$.
There are two kinds of A atoms, A' and A'':
A' in 2(*a*): 0,0,0; $\frac{1}{2},\frac{1}{2},\frac{1}{2}$;
A'' in 6(*b*): $0,\frac{1}{2},\frac{1}{2}$ *etc.*;
B in 8(*c*): $\frac{1}{4},\frac{1}{4},\frac{1}{4}$ *etc.*;
X in 24(*g*): 0,*y*,*z* *etc.*,
with $y = (3 \cos \varphi + \sqrt{3} \sin \varphi)/(8 \cos \varphi + 4)$,
$z = (3 \cos \varphi - \sqrt{3} \sin \varphi)/(8 \cos \varphi + 4)$.

If φ is allowed to increase until the next-nearest $X-X$ distance is reduced to the octahedron-edge length (the nearest $X-X$ distance) it will then be $\varphi = \cos^{-1}|(3 + \sqrt{5})/\sqrt{32}| = 22{\cdot}24°$. At this stage $y = 0{\cdot}301$ and $z =$

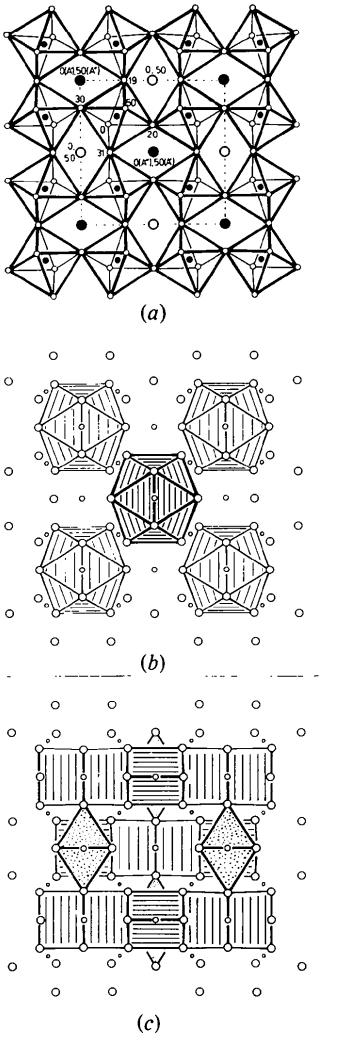

Fig. 2. (*a*) The collapsed ideal perovskite structure with space group *Im*3 ($\varphi = 22{\cdot}24°$), $A'A''_3B_4O_{12}$, projected along [001]. [Compare with Fig. 1(*a*).] Large, filled circles are A' atoms at 0,0,0, and $\frac{1}{2},\frac{1}{2},\frac{1}{2}$, and A'' atoms at $0,0,\frac{1}{2}$, and $\frac{1}{2},\frac{1}{2},0$; large, open circles are A'' atoms; small filled circles are B atoms; small open circles are X atoms. BX_6 octahedra in the lower half of the unit cell are outlined; those in the upper half are generated by a mirror plane at $z = \frac{1}{2}$. (Note also the mirror planes at $x = \frac{1}{2}$ and $y = \frac{1}{2}$.) (*b*) As (*a*), but the $A'X_{12}$ coordination icosahedra are now emphasized. (*c*) As (*a*), but now the tetracapped rhombic prisms around the A'' sites are emphasized. (In *b* and *c* the large, medium and small circles are respectively X, A and B atoms.)

0·186, and the structure is as shown in Fig. 2(*a*). The unit-cell volume has decreased by a little more than 14%.

The BX_3 arrangement is very close to that in the hydroxides of Sc, Ga and In: for $Sc(OH)_3$, $y = 0{\cdot}307$, $z = 0{\cdot}182$. Not surprisingly, the oxy-hydroxide $WO_{2{\cdot}47}(OD)_{0{\cdot}53}$ (Wiseman & Dickens, 1973) is only partly collapsed: $y = 0{\cdot}284$, $z = 0{\cdot}216$, corresponding to $\varphi = 13°$. A number of phosphides, arsenides and antimonides of the transition metals, typified by skutterudite ($D0_2$) or by $CoAs_3$, have essentially the same structure, but the anion parameters (Kjekshus & Rakke, 1974) are a little different: $y \simeq 0{\cdot}34$, $z \simeq 0{\cdot}15$, corresponding to larger rotation angles, $31° < \varphi < 36°$, a consequence of X–X bonding (Hulliger, 1968). (The octahedra are slightly distorted.)

The coordinations of the A atoms in the collapsed ($\varphi = 22{\cdot}24°$) structure are of interest (Nyman, 1976). The A' atom is surrounded by 12 equidistant X atoms at the vertices of a regular icosahedron (Fig. 2*b*), rather than the cuboctahedron of the parent structure. This transformation of a cuboctahedron into an icosahedron is well known in other contexts (Mackay, 1962; Wells, 1975). The combination of A' and X atoms has the stoichiometry $A'X_{12}$ and the structure of $A'Al_{12}$ (A' = W, Mo, Re or Tc). For these compounds $y = 0{\cdot}308$, $z = 0{\cdot}187$ (Walford, 1964), also rather close to the values for regular polyhedra.

The A'' atoms are in a site of almost square coordination: the nearest X atoms are at the corners of a rectangle with edges of $\sqrt{2}d$ and $(3 + \sqrt{32} - \sqrt{5})/\sqrt{18} = 1{\cdot}51d$. One might therefore expect the A'' site to accommodate cations such as Mn^{3+} or Cu^{2+} which have a preference for square-planar coordination and, indeed, $NaMn_7O_{12}$ has this $Im3$ structure type (Marezio, Dernier, Chenavas & Joubert, 1973), with $y = 0{\cdot}313$, $z = 0{\cdot}183$. With these parameters the rectangle is closer to a square than in the ideal case (the ratio of the sides is 1·02 instead of 1·07) and so, presumably, the Mn in the 6(*b*) site is trivalent. Other compounds with the same structure, but with Cu in the A'' site, are $CaCu_3Mn_4O_{12}$, with $y = 0{\cdot}303$, $z = 0{\cdot}182$ (Chenavas, Joubert, Marezio & Bochu, 1975), in which the octahedra are very regular but the icosahedra are slightly distorted, and $ThCu_3Mn_4O_{12}$, with $y = 0{\cdot}299$, $z = 0{\cdot}177$ (Deschizeaux, Joubert, Vegas, Collomb, Chenavas & Marezio, 1976), in which the A'' coordination is perfectly square. The cuboctahedron around A'' in the parent structure has been transformed into a tetracapped rhombic prism (Nyman, 1976), which is a pair of trigonal prisms with parallel threefold axes, sharing a square face, and with caps on each of the unshared square faces. These are emphasized in Fig. 2(*c*).

In the ideal structure (with regular octahedra) there is only one B–X–B angle, given by $\theta = \cos^{-1}[1 - 2(2 \times \cos\varphi + 1)^2/9]$, which is 143·8° in the collapsed structure ($\varphi = 22{\cdot}24°$).

Sequence (ii): structures with trigonal, $R\bar{3}c$ symmetry

The rotation axes used to derive the second hettotype are all parallel or antiparallel, so that a trigonal structure results. The operation is well known, and has been extensively and thoroughly discussed (Hepworth, Jack, Peacock & Westland, 1957; Megaw & Darlington, 1975). Here, for completeness, we give the numerical data for the structure with *regular* octahedra (Michel, Moreau & James, 1971) and a summary of the structural transformations. For a resulting hexagonal unit cell the transformation matrix is $\bar{1}01/110/222$.*

Space group $R\bar{3}c$ (No. 167; hexagonal unit cell);
$a = \sqrt{8}d\cos\varphi$, $c = \sqrt{48}d$.
Unit-cell volume $V(\varphi) = V(0)\cos^2\varphi$.
A in 6(*a*): 0,0,$\frac{1}{4}$ *etc.*;
B in 6(*b*): 0,0,0 *etc.*;
X in 18(*e*): x,0,$\frac{1}{4}$ *etc.* with $x = (\sqrt{3} - \tan\varphi)/\sqrt{12}$.

As φ increases, the next-nearest X–X distance decreases, becoming equal to the octahedron-edge length at $\varphi = 30°$, when the incomplete (75%) c.c.p. X array of the arisotype has transformed to the perfect h.c.p. array of X in the hettotype. The BX_3 array has then changed from that in ReO_3 to that in PdF_3 ($= RdF_3 = IrF_3$) *via* those of several other transition-metal trifluorides (Ti,Fe,Co,V,Cr,Ga,Mo,Ru) at intermediate rotation angles, $13° \le \varphi \le 27{\cdot}5°$. Fig. 3 shows this transformation in an unusual projection, partly in order to facilitate comparison with that due to system (iv). The monoclinic unit cell shown for ideal $\mathbf{PdF_3}$ (regular octahedra and $\varphi = 30°$) has $a/b = (11/20)^{1/2} = 0{\cdot}742$, $c/b = (9/20)^{1/2} = 0{\cdot}671$, and $\gamma = \cos^{-1}(-1/55)^{1/2} = 97{\cdot}75°$. The transformation matrix for this unit cell, in terms of the re-oriented $E2_1$ subcell, is $0\bar{1}\bar{1}/200/0\bar{1}1$.

The ABX_3 array of the ideal perovskite structure similarly transforms to that of high-temperature ($t >$

* It is convenient, here and in sequence (iv), to change the orientation of the aristotype unit cell in Fig. 1(*b*) according to the matrix 001/100/010.

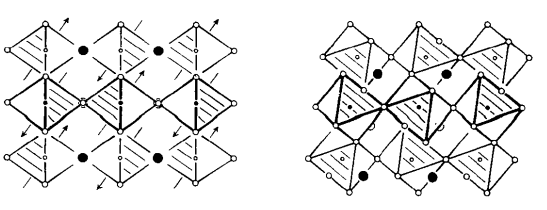

Fig. 3. The transformation of the ideal, cubic perovskite type (on the left) to the collapsed ABX_3 structure with space group $R\bar{3}c$ and $\varphi = 30°$ (on the right). [Compare Fig. 1(*b*).] Rotation axes are shown, and corresponding faces of the BX_6 octahedra are emphasized in the two cases. Note the small shuffles of the A atoms; also that, in the collapsed structure, the AX_3 and BX_3 arrays are identical. The B atoms outline one unit cell in each case: on the left it is C-centred tetragonal (c is horizontal); on the right it has become monoclinic.

1200°C), paraelectric $LiNbO_3$, with the (unshuffled) A atoms in triangular coordination (in the common face between two empty octahedra). $LaAlO_3$, $PrAlO_3$ and $NdAlO_3$ are isostructural, but with lower values of φ and some compression of the BO_6 octahedra parallel to the rotation axes. At lower temperatures the Li and Nb atoms in $LiNbO_3$ are both octahedrally coordinated: as φ increases and the Kagomé nets of anions in the parent structure collapse to triangular nets in the daughter, the A atoms originally at the centres of the hexagons are ejected into the space between the anion layers, *i.e.* into the developing octahedra; all in the same direction in the case of $LiNbO_3$. This reduces the symmetry from $R\bar{3}c$ to $R3c$. [The situation is complicated by both cations being off-centre, and octahedra being of two different sizes (Megaw, 1968).]

In the ideal, completely collapsed structure the A and B arrays are identical. Hence, if the B sites are filled but the A sites are empty, Fig. 3 represents the transformation $\mathbf{ReO_3} \rightarrow \mathbf{PdF_3}$, by the rotation of BX_6 octahedra. But, if the A sites are filled and the B sites are empty, it represents the transformation $\mathbf{AuCu_3} \rightarrow \mathbf{PdF_3}$ (= ε-Fe_3C), by the rotation of (empty) X_6 octahedra. Note that, in the latter case, a substitutional atom (**Au** in c.c.p. $\mathbf{AuCu_3}$) has been transformed continuously into an interstitial (**Pd** in h.c.p. **F**). It also follows that, formally, $\mathbf{AuCu_3}$ can be transformed to $\mathbf{ReO_3}$ by first rotating the empty octahedra and then the filled ones.

As Megaw (1968) has pointed out, increasing the rotation angle to $\varphi = 40{\cdot}09°$ transforms perovskite to the calcite structure ($G0_1$) of $CaCO_3$. No shuffling of the A atoms is necessary: in the derived structure they are C atoms in triangular coordination in the CO_3 groups. (The Ca atoms are in the B sites, and their octahedra are somewhat elongated parallel to the rotation axes, so that c/a is increased from the ideal value of 3·202 to 3·407.)

In this operation, at $\varphi = 30°$ the cuboctahedron has transformed to two face-shared octahedra, with six tetrahedra (= three trigonal bipyramids) on the re-entrant faces. In the ideal structure there is again only one B–X–B angle, given by $\theta = \cos^{-1}[(1 - 4\cos^2\varphi)/3]$, which is 131·8° in the collapsed structure ($\varphi = 30°$).

Sequence (iii): structures with tetragonal, *I*4/*mmm* symmetry

All eight possible rotation axes are now operating. For the octahedra to remain regular it is necessary that the rotation axes themselves tilt. A simple, regular way to achieve this is to eliminate an ⟨001⟩ component, and rotate about ⟨110⟩ axes. The new structure, $A'A''A_2'''B_4X_{12}$, is then expressed in terms of the rotation angle as follows.

Unit-cell transformation matrix: 200/020/002.
Space group *I*4/*mmm* (No. 139);

$a = 2d(1 + \cos\varphi)$, $c = 4d\cos\varphi$.
$V(\varphi) = V(0)\cos\varphi(1 + \cos^2\varphi)/4$.
A' in 2(*a*): 0,0,0; $\frac{1}{2},\frac{1}{2},\frac{1}{2}$;
A'' in 2(*b*): 0,0,$\frac{1}{2}$; $\frac{1}{2},\frac{1}{2}$,0;
A''' in 4(*c*): 0,$\frac{1}{2}$,0; $\frac{1}{2}$,0,0; $\frac{1}{2}$,0,$\frac{1}{2}$; 0,$\frac{1}{2},\frac{1}{2}$;
B in 8(*f*): $\frac{1}{4},\frac{1}{4},\frac{1}{4}$ *etc.*;
X' in 8(*h*): $x,x,0$ *etc.*,
with $x = (1 + \cos\varphi + \sqrt{2}\sin\varphi)/(4 + 4\cos\varphi)$;
X'' in 16(*n*): $0,y,z$ *etc.*,
with $y = 1/(2 + 2\cos\varphi)$, $z = (\sqrt{2} - \tan\varphi)/(4\sqrt{2})$.

The fully-collapsed structure (next-nearest X–X distance equal to the octahedron-edge length) occurs for $\varphi = \sin^{-1}(\frac{1}{3}) = 19{\cdot}47°$. It is shown in Fig. 4. At this point the A' atoms are at the centres of regular cubes of X'' atoms, four lateral faces of which are capped by X' atoms; and the A'' atoms are at the centres of the common faces between pairs of (square-) face-sharing, square antiprisms. The cubes and antiprisms together form columns by face-sharing along [0,0,z] and [$\frac{1}{2},\frac{1}{2}$,z], the repeat unit being a pair of antiprisms and a cube, see Fig. 5. [The antiprisms are very slightly distorted; one square face (X_4') has edges about 4% longer than

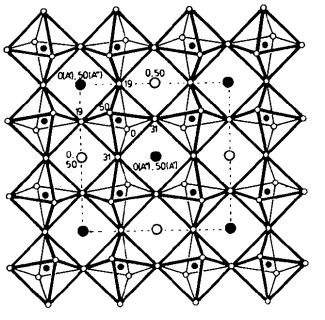

Fig. 4. The collapsed perovskite structure $A'A''A_2'''B_4O_{12}$, with space group *I*4/*mmm* and $\varphi = 19{\cdot}47°$, projected along z. [Compare Figs. 1(*a*) and 2(*a*).] Again, the upper half of the unit cell is generated by a mirror plane at $z = \frac{1}{2}$. The B atoms are at $z = \frac{1}{4}$: the large open circles are A''' atoms; the large filled circles are A' and A''.

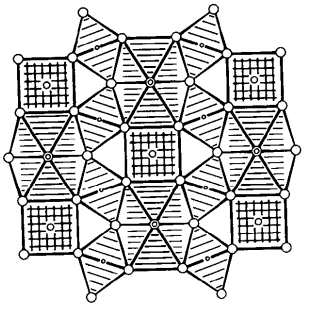

Fig. 5. A bounded projection of half the *I*4/*mmm* structure on {110} showing the columns of BX_6 octahedra, and $A'X_8$ cubes and $A''X_{12}$ pairs of square antiprisms parallel to z.

those of the other (X_4'').] Thus, half of the cuboctahedra in the aristotype have been changed by alternate compression and extension along the fourfold axes parallel to **c**. The coordination of the A''' atoms is less regular. It may perhaps be best described as distorted tetracapped rhombic prisms, or as icosahedra that have been compressed along twofold axes to produce some re-entrant faces [*cf.* (i) above].

The structures of $NaSb(OH)_6$, $AgSb(OH)_6$ and $FeGe(OH)_6$ (stottite) are related,* but reduced in symmetry to space group $P4_2/n$ because of the ordering of the two types of cations on the B sites. (All the A sites are empty, and the H positions are unknown.) A number of ternary fluorides, *e.g.* $KZnF_3$, have been reported to be tetragonal with $c/a < 1$ and with a and c approximately twice the unit-cell edge of the aristotype (Ludekens & Welch, 1952). It is possible that these compounds have this $I4/mmm$ structure.

There are now two B–X–B angles: for B–X'–B, $\theta' = \cos^{-1}(1 - 2\cos^2\varphi)$, which is 141·1° for $\varphi = 19{\cdot}47°$; and, for B–X''–B, $\theta'' = \cos^{-1}[1 - (1 + \cos\varphi)^2/2]$, which is 152·5° for $\varphi = 19{\cdot}47°$.

Sequence (iv): structures with orthorhombic, *Pnma* symmetry

The last group of operations involves rotation axes in the $(0\bar{1}1)$ plane of the parent structure (using the convention of Table 1). It is less often discussed, but perhaps the most interesting and important of the four. The space group of the derived structure is *Pnma*, with the rotation axes in the (001) plane of the new, orthorhombic unit cell. Perfect regularity of the octahedra is again incompatible with fixed rotation axes: a primary rotation of φ demands a secondary tilt (of the octahedra and the primary axes) of $\pm\psi$ about an axis [001] of the orthorhombic cell normal to the first. For regular octahedra $\psi = \tan^{-1}[\sqrt{2}(1 - \cos\varphi)/(2 + \cos\varphi)]$ so that, for example, $\varphi = 15$, 30° means $\psi =$ 0·93, 3·78° respectively. [An analogous second rotation was needed in developing an orthorhombic structure from the cubic $C9$ type (O'Keeffe & Hyde, 1976).] In what follows it is assumed that the second tilt or rotation is made. The unit-cell transformation matrix is $0\bar{1}\bar{1}/200/0\bar{1}1$ [as for the $R\bar{3}c$ monoclinic cell in (ii)].

Space group *Pnma* (No. 62);
$a = d[8(2 + \cos^2\varphi)/3]^{1/2}$,
$b = d[48/(1 + 2\sec^2\varphi)]^{1/2}$,
$c = d\sqrt{8}\cos\varphi$.
$V(\varphi) = V(0)\cos^2\varphi$.
A in 4(c): $x,\frac{1}{4},z$ *etc.*,
with $x = z = 0$ (if there are no shuffles, see below);
B in 4(b): $0,0,\frac{1}{2}$ *etc.*;
X' in 4(c):
with $x = (\cos^2\varphi - 1)/(2\cos^2\varphi + 4)$,
$z = (\sqrt{3} + \tan\varphi)/\sqrt{12}$;
X'' in 8(d): x,y,z *etc.*,
with $x = (2 - \sqrt{3}\sin\varphi\cos\varphi + \cos^2\varphi)/(8 + 4\cos^2\varphi)$,
$y = -(\tan\varphi)/\sqrt{48}$,
$z = (3\sqrt{3} + \tan\varphi)/\sqrt{48}$.

If the octahedra are perfectly regular, then φ can be determined directly from the lattice parameters by $\varphi = \cos^{-1}|\sqrt{2}c^2/(ab)|$. But this is often not the case (and the value of φ so calculated is very sensitive to even small distortions). It is best determined from the value of $y(X'')$. (A difference between the two values indicates distortion of the unit cell and octahedra; *cf.* the case of YF_3 below.)

The derived structure for $\varphi = 30°$ is shown in Fig. 6. (As ψ is much less than φ, only the principal rotation axes are shown.) Comparison with Fig. 3 reveals that the new orthorhombic unit cell is equivalent to the monoclinic cell of $\mathbf{PdF_3}$; the cell angle has changed from 97·75 to 90°. The axial ratios of the new cell are $a/b = (81/152)^{1/2} = 0{\cdot}730$, $c/b = (9/19)^{1/2} = 0{\cdot}689$, which values may be compared with those given above for the ideal, monoclinic cell of $\mathbf{PdF_3}$. The differences are rather small.

Again there are two B–X–B angles: for B–X'–B, $\theta' = \cos^{-1}|(2 - 5\cos^2\varphi)/(2 + \cos^2\varphi)|$, which is 129·5° for $\varphi = 30°$; and, for B–X''–B, $\theta'' = \cos^{-1}|(1 - 4\cos^2\varphi)/3|$, which is 131·8° for $\varphi = 30°$.

The value of φ at which next-nearest X–X distances become equal to the octahedron-edge length is less than 30°, and given by $\varphi = \tan^{-1}(\sqrt{3}/4) = 23{\cdot}41°$ (when $\psi = 2{\cdot}29°$). At higher angles there is a shorter X–X distance across the mirror plane: $\sqrt{2}(\sqrt{3} - \tan\varphi)/(1 + 2\sec^2\varphi)^{1/2}$ which, when $\varphi = 30°$, is $(8/11)^{1/2} = 0{\cdot}853$ times the octahedron-edge length.

The coordination polyhedron about the A atom in the collapsed structure is a slightly distorted, bicapped trigonal prism. When the rotation angle is less than 30° it is tapered, one triangular face being larger than the other. At $\varphi = 23{\cdot}41°$ one face is square – that normal to the mirror plane. At $\varphi = 30°$ it is a right prism, and two faces are square: the face normal to the mirror plane is now rectangular because of the short X–X

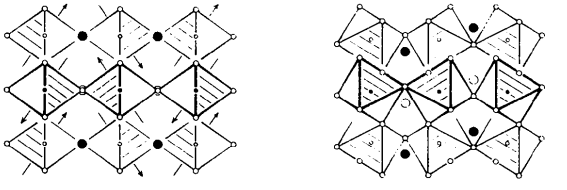

Fig. 6. Derivation of the ideal ($\varphi = 30°$), collapsed *Pnma* structure from perovskite (analogous to Fig. 3), projected on (001). Again, the B atoms outline one unit cell; the (primary) rotation axes are shown; and the small shuffles of the A atoms should be noted.

* We are grateful to Sten Andersson for pointing this out to us.

distance already referred to. The A atoms become more nearly equidistant from the X atoms at the corners of the trigonal prism if their x and z parameters are allowed to become slightly positive; a shift analogous to that in (ii).

There are very many compounds with this hettotype structure. Perovskites with *Pnma* symmetry are numerous, and include the mineral perovskite, $CaTiO_3$ itself. The type compound is gadolinium ferrite, $GdFeO_3$ (Geller, 1956; Coppens & Eibschütz, 1965), one of the lanthanoid orthoferrites, $LnFeO_3$ (Marezio, Remeika & Dernier, 1970), which provide a sequence across a range of rotation angles from $\varphi = 15°$ for $LaFeO_3$ (Marezio & Dernier, 1971) to $\varphi = 23°$ for $LuFeO_3$. The structures of two well-separated members of the series are shown in Fig. 7. These may be compared with Fig. 6: note particularly the differences in the rotation angles, as indicated by the different orientations of the octahedra. Data for these compounds are included in Table 2: close agreement between the two calculated values of φ for a given compound indicates very small distortions of the FeO_6 octahedra. Marezio & Dernier (1971) have pointed out that these distortions increase with increasing size of the lanthanoid ion, and this is reflected in the increasing discrepancy between the two φ values. But, it should be added, the distortion is still not large even in the case of $LaFeO_3$, for which the octahedron-edge lengths are 2·803, 2·843 and 2·858 Å.

Many other oxides, having Al, Sc, Cr, Ga, Co, V or Rh in place of Fe are isostructural with $GdFeO_3$, as well as some sulphides such as $UCrS_3$ (Noël, Padiou & Prigent, 1975) with U in the A sites, $BaUS_3$ (Brochu, Padiou & Grandjean, 1970) with U in the B sites, $YScS_3$ (Rodier & Laruelle, 1970), and halides such as, probably, neighbourite, $NaMgF_3$ (Chao, Evans, Skinner & Milton, 1961).

In general, the parameters of the A atoms increase with increasing φ (*cf.* especially the **$GdFeO_3$** compounds in Table 2), but there are some notable

Table 2. *Pnma structures; parameters and deduced rotation angles, φ*

			X'		X''							
Structure	x	z	$-x$	z	x	$-y$	z	a/b	c/b	φ_1[c]	φ_2[d]	Reference
Ideal (cubic) perovskite	0	0	0	$\frac{1}{2}$	$\frac{1}{4}$	0	$\frac{3}{4}$	$1/\sqrt{2}$	$1/\sqrt{2}$	0°	0°	–
Ideal collapsed, 1[a]			$\frac{1}{36}$ 0·028	$\frac{5}{8}$ 0·625	$\frac{7}{36}$ 0·194	$\frac{1}{16}$ 0·063	$\frac{13}{16}$ 0·813	$9/\sqrt{152}$ 0·730	$3/\sqrt{19}$ 0·688	23·41	23·41	–
Ideal collapsed, 2[b]			$\frac{1}{22}$ 0·046	$\frac{2}{3}$ 0·667	$\frac{2}{11}$ 0·182	$\frac{1}{12}$ 0·083	$\frac{5}{6}$ 0·833	$11/\sqrt{216}$ 0·749	$\sqrt{66}/12$ 0·677	30·00	30·00	–
$ScCoO_3$	0·023	−0·017	0·072	0·679	0·183	0·078	0·866	0·781	0·662	28	37	1
$TeCoO_3$	0·010	−0·013	0·050	0·663	0·183	0·066	0·866	0·801	0·709	24	27	1
$LuFeO_3$	0·071	0·020	0·046	0·620	0·193	0·062	0·811	0·733	0·689	23	24	2
$GdFeO_3$	0·063	0·016	0·033	0·601	0·198	0·051	0·804	0·732	0·698	19	20	2
$PrFeO_3$	0·044	0·009	0·021	0·582	0·208	0·044	0·792	0·716	0·704	17	12	2
$LaFeO_3$	0·028	0·006	0·012	0·573	0·218	0·039	0·781	0·707	0·706	15	5	3
$SrZrO_3$	0·025	0·001	0·015	0·573	0·215	0·035	0·784	0·710	0·706	14	7	4
$CaTiO_3$	0·030	0·000	01018	0·537	0·232	0·026	0·768	0·712	0·703	10	11	5
$UCrS_3$	0·118	0·052	0·042	0·641	0·171	0·059	0·832	0·809	0·689	22	34	6
Pd_3B	0·116	0·067	0·037	0·655	0·180	0·070	0·828	0·722	0·641	26	36	7
Fe_3C	0·123	0·056	0·037	0·660	0·182	0·067	0·837	0·755	0·671	25	32	8
Ni_3B	0·104	0·072	0·026	0·630	0·180	0·062	0·845	0·787	0·664	23	38	9
$NiAl_3$	0·131	0·055	0·011	0·585	0·174	0·053	0·856	0·898	0·653	20	47	10
Pd_3Si	0·103	0·031	0·005	0·596	0·181	0·051	0·822	0·759	0·696	19	25	11
TlF_3	0·131	0·040	0·038	0·624	0·169	0·074	0·837	0·829	0·691	27	36	12
$BiCl_3$	0·047	0·023	0·057	0·652	0·176	0·067	0·854	0·833	0·686	25	37	13
YF_3	0·133	0·058	0·028	0·601	0·165	0·060	0·863	0·927	0·641	23	51	14
	0·133	0·059	0·023	0·591	0·165	0·064	0·876	0·927	0·641	24	51	15
LaF_3[e]	0·167	0·000	0·000	0·500	0·167	0·07	0·000	0·977	0·564	26	63	16

(*a*) Regular octahedra, and the shortest $X-X$ distance between adjacent octahedra equal to the octahedron-edge length.
(*b*) Regular octahedra, and $\varphi = 30°$, so that the shortest $X-X$ distance is $(8/11)^{1/2}$ times the octahedron-edge length.
(*c*) $\varphi_1 = \tan^{-1}|-y(X'')\sqrt{48}|$.
(*d*) $\varphi_2 = \cos^{-1}|\sqrt{2c^2/(ab)}|$.
(*e*) True symmetry hexagonal (see text).

References: (1) Kohn, Inoue, Horie & Akimoto (1975). (2) Marezio, Remeika & Dernier (1970). (3) Marezio & Dernier (1971). (4) Ahtee, Ahtee, Glazer & Hewat (1976). (5) Kay & Bailey (1957). (6) Noël, Padiou & Prigent (1975). (7) Stenberg (1961). (8) Fasiska & Jeffrey (1965). (9) Rundqvist & Pramatus (1967). (10) Schubert (1964). (11) Aronsson & Nylund (1960). (12) Hebecker (1972). (13) Nyburg, Ozin & Szymański (1971). (Data adapted from those for space group $Pn2_1a$.) (14) Zalkin & Templeton (1953). (15) Cheetham & Norman (1974). (16) Schlyter (1952).

exceptions. The selenates of Mg, Mn, Co, Ni and Zn (Kohn, Inoue, Horie & Akimoto, 1975) are almost completely collapsed, $27° \leq \varphi \leq 30°$, but the atom parameters of Se are very low. A similar situation obtains in the structure of $TeCoO_3$ (Kohn *et al.*, 1975): $\varphi = 24°$. Clearly the *A* atoms are displaced to one end of the trigonal prism, the cause being the stereochemically active lone pair of electrons on Se^{IV} and Te^{IV} (Table 2).

Of at least equal interest is the derived structure when the parent is AX_3 (**$AuCu_3$**), rather than ABX_3. It is rather important, being the $D0_{11}$ type of cementite, Fe_3C (Fasiska & Jeffrey, 1965), for which $\varphi = 25°$. This value lies between the two 'ideal' values calculated above, and this is reflected in the characteristic short Fe–Fe distance across the mirror plane (2·475 Å, compared with the average of 2·664 ± 0·014 Å for the other edges of the trigonal prism). The structure is shown in Fig. 8.* It has previously been described (Andersson & Hyde, 1974; Hyde, Bagshaw, Andersson & O'Keeffe, 1974) as 'chemically twinned' or 'unit-cell-twinned' h.c.p. Fe with C atoms in the twin/composition planes which, in this case, are the mirror planes at $y = \pm\frac{1}{4}$. Comparison of Fig. 3 on the one hand with Figs. 6 and 8 on the other confirms this description: the *X* atoms in **PdF_3** are hexagonally close-packed, and 'ideal' **Fe_3C** (Fig. 6) is simply **PdF_3** with alternate (010) lamellae (monoclinic unit cell) in a twin orientation; adjacent lamellae being joined at the mirror planes. That is, **Fe_3C** is **PdF_3** mimetically twinned on the finest possible scale that retains the empty octahedra. This relation is, in fact, implicit in the two relevant vector sets [(ii) and (iv)] in Table 1: the upper rows of each set are identical; the lower rows are related by a reflection in the (100) plane of the aristotype, which is (010) of both hettotypes (*cf.* the transformation matrices given earlier). The $GdFeO_3$ structure is related to that of high-temperature $LiNbO_3$ in exactly the same way. Except for a smaller tilt angle (~8°), the structure of the $NaNbO_3$ phase *P* (Sakowski-Cowley, Łukaszewicz & Megaw, 1969) is similarly related to $LiNbO_3$, but now the twin bands are twice as wide. (Transformation mechanisms are discussed below.)

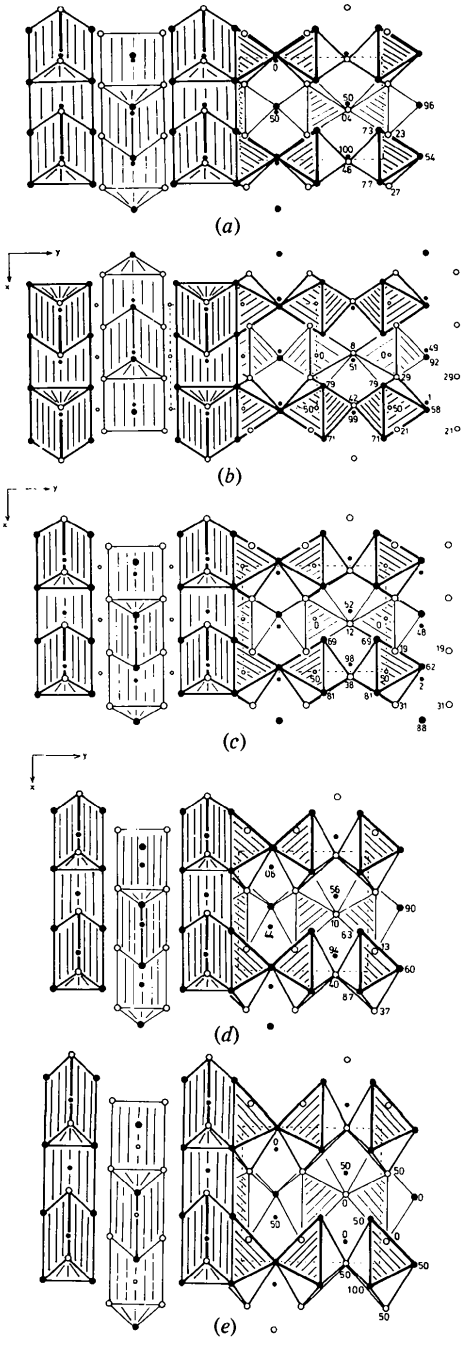

Fig. 7. Projections on (001) of the *Pnma* (or equivalent) unit cell, analogous to Fig. 6 but with smaller rotation angles, φ: (*a*) $CaTiO_3$, (*b*) $PrFeO_3$, (*c*) $LuFeO_3$, (*d*) YF_3, (*e*) LaF_3.

* It is an odd fact that the structures of both $GdFeO_3$ and Fe_3C are almost never projected in the particular direction used here, although it seems to depict them most clearly. This is even more surprising since it is also the projection down the shortest axis of the unit cell, and the cardinal rule is (almost) always to project down the shortest axis.

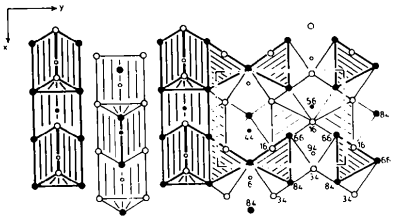

Fig. 8. Cementite, Fe_3C, projected on (001) [*Pnma*]. (Compare Figs. 6 and 7.)

Comparison of the two descriptions of the Fe_3C structure also illustrates rather clearly the need for the second tilt angle ψ. Thus, starting from the ReO_3 structure, rotations by $\varphi = 30°$ according to sequence (ii) produce the PdF_3 structure (interstitial **Pd** in h.c.p. **F**). Twinning on $(11\bar{2}2)$ of this ideal $[c/a = (8/3)^{1/2}]$ h.c.p. unit cell results in the rotation axes ($\langle 0001 \rangle$ of the hexagonal structure) in each twin being inclined to each other by $\cos^{-1}(5/11) = 62{\cdot}96°$. On the other hand, starting from the substitutional alloy structure of $AuCu_3$, the rotation axes of sequence (iv) are $\pm[111]$ and $\pm[\bar{1}11]$ which are inclined to each other by $\cos^{-1}(1/3) = 70{\cdot}53°$. The difference between these two angles is just 2ψ ($= 7{\cdot}57°$ for $\varphi = 30°$).

The structure reported for $NiAl_3$ (Bradley & Taylor, 1937) is Fe_3C, except that the rotation angle is smaller, $\varphi = 20°$, and the octahedra less regular (compare the two calculated φ values in Table 2). The parameters for the A atoms are almost the same in the two structures (rather higher than for $GdFeO_3$, a difference not obviously accountable for). A number of carbides, borides and silicides are isostructural, and also alloys of Co or Ni with the lanthanoids, $CoLn_3$ and $NiLn_3$.* All these are therefore rather simply related to the $AuCu_3$ type: another direct geometrical connection between substitutional and interstitial alloy structure types.

A number of metal trifluorides occur with the antitype structure including TlF_3, BiF_3 and, with elongated a axes and distorted octahedra, YF_3 and a number of other lanthanoid trifluorides. The structure of YF_3 is included in Fig. 7. In the structure of $BiCl_3$ the x and z parameters of the A atoms are rather low for the calculated φ value that obtains. [In Table 2 compare x and z for Bi in $BiCl_3$ with those for Tl in TlF_3 (Hebecker, 1972).] The explanation is as in the cases of *Pnma* selenates and tellurates already discussed: a stereochemically active lone pair of electrons on Bi^{3+} pushes this atom towards one end of the trigonal prism. Isostructural compounds not surprisingly include $SbCl_3$ and β-$SbBr_3$.

A perennial problem in many of these structures is doubt about the exact symmetry and space group, *Pnma* or $Pna2_1$, and occasionally incontrovertible evidence for the (latter) lower symmetry. However, even in these latter cases, the structure is not significantly affected geometrically by the alternative choice. $BiCl_3$ is a case in point: the correct space group is $Pna2_1$, but the derived coordinates are virtually the same in both space groups. (Those in Table 2 are derived from the values in the setting $Pn2_1a$.)

Finally, although ideal perovskite is normally regarded as a 'filled' ReO_3 type, it is equally legitimate to describe it as a filled $AuCu_3$ type; which suggests the possibility of filling Fe_3C in ways other than by putting

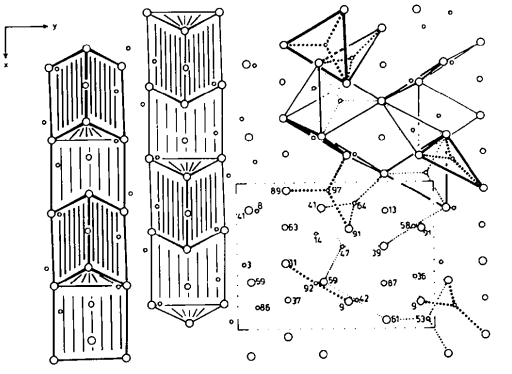

Fig. 9. The low-temperature, $P2_12_12_1$ structure of wittichenite, $BiCu_3S_3$, projected on (001). Large circles are S atoms, medium circles are Bi and small circles are Cu. On the left the BiS_6 trigonal prisms are shown. (Note their slight distortion – the absence of the mirror plane of *Pnma*.) In the top right, CuS_3 triangles are outlined. (They define the S_6 octahedra fairly clearly.) Some Cu–S bonds are indicated by dotted lines. The unit cell is outlined by the broken lines at the bottom right.

B atoms into the octahedra. This occurs, for example in wittichenite, $BiCu_3S_3$ (Kocman & Nuffield, 1973) shown in Fig. 9. The AX_3 array is BiS_3, and the Cu atoms are in threefold coordination. This is the low-temperature structure which, although orthorhombic, has space group $P2_12_12_1$; reduced from *Pnma*, clearly by the specific ordering pattern of the Cu. However, above 150°C the space group is *Pnma*, presumably because the Cu atoms are now disordered (Karup-Møller & Makovicky, 1974), a common occurrence in many copper sulphides including chalcocite, Cu_2S (Buerger & Wuensch, 1963). Skinnerite, $SbCu_3S_3$, is similar to wittichenite, although the low-temperature form ($t < 122$°C) is now monoclinic, space group $P2_1/c$, with a doubled c axis (Karup-Møller & Makovicky, 1974).*

Further consideration of the rare-earth trifluoride structures

In the previous section we remarked on the topological identity of the YF_3 and Fe_3C structures, and elsewhere (O'Keeffe & Hyde, 1975) we have commented on the similarity between the structures of YF_3 and tysonite ($D0_6$), LaF_3. There are more than 50 compounds with the tysonite or anti-tysonite structure, and so it is inevitable that it should be reconsidered in the present context. The result is illuminating.

Details of the LaF_3 structure have been the subject of controversy. A very simple, high-symmetry ($P6_3/mmc$)

* It is interesting that in different compounds lanthanoid atoms can occupy the three different sites A, B and X of the $E2_1$ aristo- and hetto-types.

* One of us would like to acknowledge a useful discussion of some mineral sulpho-salt structures with E. Makovicky of the Mineralogy–Geology Institute of Copenhagen University, who drew our attention to these last two compounds.

structure has been proposed (Schlyter, 1952), with a = 4·148, c = 7·354 Å, La in 2(*c*): $\pm(\frac{1}{3},\frac{2}{3},\frac{1}{4})$, F(1) in 2(*b*): $\pm(0,0,\frac{1}{4})$, and F(2) in 4(*f*): $\frac{1}{3},\frac{2}{3},u$ *etc.* with u = 0·57. This is the antitype, with almost the same values of c/a and u, of the structure originally proposed for Na_3As and isostructural compounds ($D0_{18}$), of which there are at least 20 (Brauer & Zintl, 1937). Other studies of LaF_3 (Oftedal, 1929, 1931; Zalkin & Templeton, 1953; Mansmann, 1965) have indicated a larger unit cell ($a' = \sqrt{3}a$) and lower symmetry, but there is disagreement about the space group and about the details of the structure. There is a similar lack of agreement about the details of some antistructural compounds such as ('$D0_{21}$') Cu_3P (Schlenger, Jacobs & Juza, 1971; Olofsson, 1972). However, all the proposed structures differ only slightly (in the details of the X_3 array) from the simple one described above; and so we consider only that one here.

Adoption of the orthohexagonal cell related to the small hexagonal cell (or subcell) by $\bar{1}10/001/110$ facilitates comparison with $\mathbf{YF_3}$. Relevant atom coordinates appropriate to this cell are included in Table 2; and the structure is shown, projected on (001) of the same cell [$\equiv (11\bar{2}0)_{hex}$], in Fig. 7 – for comparison with those of $CaTiO_3$, $PrFeO_3$, $LuFeO_3$ and YF_3.

The five structures provide a striking example of what has been described as the continuity between structure types (Hyde, Bursill, O'Keeffe & Andersson, 1972). Starting from the anion array of $E2_1$ or $D0_9$, rotation of essentially regular octahedra produces that in the orthorhombic perovskite sequence, with $\mathbf{CaTiO_3}$ and $\mathbf{PrFeO_3}$ as intermediate cases and $\mathbf{LuFeO_3}$ as an example of a virtually completely collapsed structure. Further evolution of the anion arrangement involves distortion of the octahedra without further rotation (*cf.* φ_1 and φ_2 in Table 2). The distortion involves compression along a threefold axis, so that the octahedron, together with an additional anion capping each of the larger faces, has become more nearly a cube; and an alternative description of this structure type is now as twinned primitive cubic packing of the X atoms (Hyde *et al.*, 1974).

This last evolutionary stage is perhaps better appreciated by concentrating on the AX_6 trigonal prisms which, in the sequence $\mathbf{CaTiO_3}$ to $\mathbf{LaF_3}$, become elongated and have their 'threefold' axes tilted out of (001) by a progressively greater amount. [Note that in the case of LaF_3, in order to facilitate the comparison with $\mathbf{YF_3}$, only 6 of the 11 near neighbours are picked out to form a trigonal prism in Fig. 7(*d*). We return to the La coordination polyhedron below.]

The atom parameters of the rare-earth fluorides isostructural with YF_3 have not yet been determined, but a consideration of their lattice parameters is informative. [For a recent compilation see Sobolev, Garashina, Fedorov & Seiranyan (1974).] Let α, β, γ be the reduced cell-edges, respectively a, b and c divided by the cube root of the unit-cell volume. Examination of

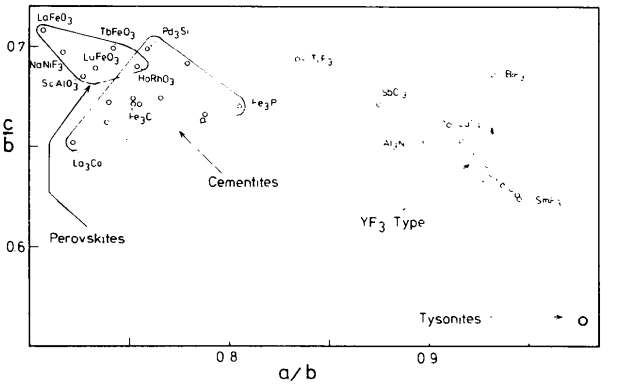

Fig. 10. The relation between c/b and a/b for the *Pnma* (or equivalent) unit cells of the structures of some compounds related to perovskite collapsed by sequence (iv). (For the ideal, cubic perovskite $c/b = a/b = 1/\sqrt{2} = 0{\cdot}707$.)

their values shows that in the sequence of increasing volume, from LuF_3 to SmF_3, α increases smoothly, β is very nearly constant, and γ decreases smoothly. Thus, the change in the shape of the unit cell may be measured by the change in the axial ratios a/b and c/b. These ratios for the $\mathbf{YF_3}$-type compounds are included in Fig. 10, and the smooth increase in a/b and decrease in c/b with increasing size of the cation may be seen. Also shown is the corresponding point for the orthorhombic unit cell of the tysonites, which all have very nearly the same cell shape (*cf.* O'Keeffe & Hyde, 1975). This last point falls very close to an extrapolation of the $\mathbf{YF_3}$ data, emphasizing that the tysonite structure is a natural evolution of the $\mathbf{YF_3}$ structure once a sufficiently large cation size is reached. Also shown in the figure are similar lattice-parameter data for *Pnma* **perovskites** and **cementites**, which have more nearly regular octahedra, and are therefore separated from the trifluorides in the axial-ratio plot.

Cation coordination in LaF_3

In $\mathbf{YF_3}$ and $\mathbf{LaF_3}$ (and the other *Pnma* structures) the coordination polyhedron of the A atom involves more than the six X atoms in the trigonal prisms outlined in Fig. 7. In $\mathbf{YF_3}$ two additional anions cap two of the 'square' faces; in $\mathbf{LaF_3}$ the number of additional capping anions is five. The increasing coordination number of the cation as its size increases provides a basis for understanding the corresponding elongation of the trigonal prisms in the sequence $\mathbf{LuFeO_3 \rightarrow LaF_3}$ (Fig. 7), as illustrated by the following simple calculation.

Consider a trigonal prism of 'point charge' anions around a central cation, subject to the constraints of (*a*) fixed cation–anion distance and (*b*) maintaining threefold symmetry. The shape of the trigonal prism is

specified by η, equal to the ratio of its height to the edge of the equilateral triangle. The minimum electrostatic energy for such a configuration is readily found to occur for $\eta = 0.916$. Now consider a similar coordination figure, but with each of the three rectangular faces of the prism capped by an additional anion, all nine anions being equidistant from the central cation. The minimum electrostatic energy is now at $\eta = 1.264$. Finally, for a 'hexacapped' prism, with six capping anions in a plane normal to the threefold axis (two to each rectangular face) the equilibrium configuration has the anions at the vertices of a twinned cuboctahedron, and $\eta = 1.633$. These figures suggest that, even if the constraints are relaxed, an increase in cation size, which leads to an increase in the coordination number of the cation, must cause an elongation of the trigonal prism which, equally inevitably, leads to the observed changes in the axial ratios of the (orthorhombic) unit cell.

However, it is logical to enquire why the changes in the sequence (say) $\mathbf{TlF_3} \rightarrow \mathbf{LaF_3}$ should be different from those in the sequence $\mathbf{LuFeO_3} \rightarrow \mathbf{LaFeO_3}$; *i.e.* why is $\mathbf{LaF_3}$ not simply $\mathbf{AuCu_3}$? The answer comes from a consideration of the coordination of the X atoms. The X coordination in a fully, or almost fully, expanded ABX_3 structure is quite regular – an A_4B_2 octahedron. But, in the AX_3 case (the B atoms being absent) it is A_4 square planar: unfavourable for electrostatic bonding and/or for covalent bonding using sp^3 hybrid orbitals on the X atoms. The drawing of the LaF_3 structure in Fig. 7 clearly shows the appropriateness of the anion coordinations therein: triangular for the X atoms in 4(*c*) and tetrahedral for those in 8(*d*). Thus, unlike the situation in $\mathbf{AuCu_3}$, in $\mathbf{LaF_3}$ both anions and cations have suitable coordination polyhedra.

Mechanisms for transforming one collapsed structure into another

A trivial consequence of the above analysis is that the hettotypes may be interconverted *via* the aristotype. But more direct mechanisms may also be envisaged.

A comparison of Figs. 3 and 6 reveals a very simple mechanism by which $\mathbf{PdF_3}$ and $\mathbf{Fe_3C}$ may be interconverted: rotate the octahedra in the central (010) lamellae (*i.e.* in alternate lamellae) about their body diagonals parallel to [010]. This relation is also implicit in the vector sets (ii) and (iv) in Table 1: the upper rows are identical (as was pointed out earlier) and all the corresponding pairs of vectors in the lower rows, in addition to being related by reflection in (100) of the aristotype, differ by $\pm[200]$. If the orientation of the aristo- and hetto-type unit cells is appropriate* then the difference is $\pm[200]_a \rightarrow \pm[010]_h$; which means that the two structures may be interconverted by rotating those octahedra corresponding to the vectors in the lower rows (B atoms at $z_a = 1$) clockwise or anticlockwise about $[100]_a \equiv [010]_h$. {In case (iv) this last vector is only approximately $[010]_h$, because $\psi \neq 0$; *cf.* Fig. 6.} (An analogous correspondence between the structures of α- and β-cristobalite was pointed out in the earlier paper.)

Similar relations between the other pairs of vector sets obviously imply the possibility of analogous mechanisms.

A second possible mechanism for transforming $\mathbf{PdF_3}$ to $\mathbf{Fe_3C}$ employs a simple twinning shear operation on alternate (010) lamellae of octahedra. The analogous production of a single $\mathbf{Fe_3C}$ lamella in a (twinned) $\mathbf{PdF_3}$ matrix may be visualized from the (001) projection and (010) section of the resulting structure in Fig. 11. The same operation, $\frac{1}{3}[\bar{1}\bar{1}23](11\bar{2}2)$ (indices of the small, h.c.p. subcell), has been described by Hirthe & Lothe (1968) for slip and deformation twinning in h.c.p. metals ($\equiv \mathbf{PdF_3}$, but with all the octahedra empty): compare their Fig. 11-7 with our Fig. 11(*b*). For $\mathbf{PdF_3}$ the twinning elements are the undistorted composition/twin plane, $K_1 = (010) \equiv (11\bar{2}2)_{h.c.p.}$; the shear direction $\eta_1 = [\bar{1}00] \equiv [\bar{1}\bar{1}23]_{h.c.p.}$; $K_2 = (\bar{1}10) \equiv (0001)_{h.c.p.}$; $\eta_2 = [110] \equiv [\bar{1}100]_{h.c.p.}$. If the A and B sites are both filled, then the same transformation corresponds to idealized $\mathbf{LiNbO_3}$ → ideal ($\varphi = 30°$) $\mathbf{GdFeO_3}$; and it is significant that exactly this operation is observed to operate in the production of both growth twins and mechanical twins in real $LiNbO_3$ crystals (Blistanov, Nosova & Tagieva, 1975). In this last case the structure of the composition plane was not clearly

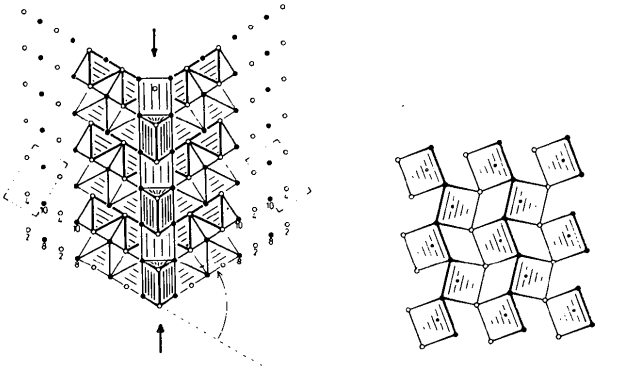

(*a*) (*b*)

Fig. 11. (*a*) The production of a single lamella (arrowed) of the *Pnma* X_3 array (ideal, $\varphi = 30°$) by mechanical twinning of h.c.p. X. The projection is on (001) of *Pnma* (as in the earlier figures), equivalent to $(1\bar{1}00)$ of h.c.p. The shear angle is indicated in the lower right. Octahedra in the twins, and trigonal prisms in the twin/composition plane, are emphasized. (*b*) The layer of trigonal prisms in the composition plane of (*a*) projected along the normal to the layer, *i.e.* the normal to $(11\bar{2}2)$ or $(1\bar{1}2\bar{2})$ of h.c.p., equivalent to (010) of *Pnma*.

* *I.e.* with the alternative orientation of the arisototype cell axes introduced earlier; transforming the cell in Fig. 1 by 001/100/010.

described, but it seems plausible that it is a unit lamella ($b/2$ thick) of $\mathbf{GdFeO_3}$ between the $LiNbO_3$ twin individuals. [Compare Fig. 11(*a*) with Fig. 4 of Blistanov *et al.* (1975) and the description of the structure of $NaNbO_3$, phase *P*, given above (sequence iv).]

Some other rotation derivatives

We have shown how the structures of some interstitial alloys may be produced from the structure of the substitutional alloy $\mathbf{AuCu_3}$ by rotating the empty X_6 octahedra about threefold axes. The number is increased by considering rotations about fourfold axes, in particular, in Glazer's (1972) notation, (v) $a^0a^0c^+$ and (vi) $a^0a^0c^-$. The rotation patterns are evident from the [001] projections of the 'completely collapsed' ($\varphi = 15°$) structures shown in Figs. 12 and 13. (Glazer has discussed the analogous 'perovskites'.)

In (v) the $\mathbf{CoGa_3}$-type AX_3 structure is produced if, at $\varphi = 15°$, the c/a ratio is reduced by a factor of $\sqrt{2}$. The [001] strings of corner-sharing octahedra then become strings of face-sharing, body-centred cubes. The cuboctahedron has collapsed to a tetracapped rhombic prism, but the Co atoms move off centre – in opposite senses in alternate layers, thus doubling the *c*-axis – to achieve bicapped, trigonal prismatic coordination.

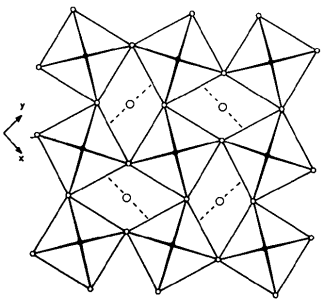

Fig. 12. The (001) projection of the ideal perovskite structure collapsed by sequence (v): octahedra rotated about ±[001]; layers identical.

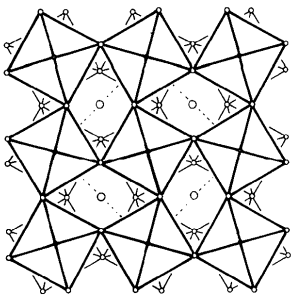

Fig. 13. The (001) projection of the ideal perovskite type structure collapsed by sequence (vi): octahedra rotated about ±[001] in alternate senses in alternate layers. (Compare Fig. 12.)

In (vi) the AX_3 derivatives are $\mathbf{U_3Si}$ at $\varphi = 4{\cdot}4°$, $\mathbf{Ir_3Si}$ at $\varphi = 14{\cdot}6°$ and, with a slight monoclinic distortion, $\mathbf{Pt_3Ge}$ and $\mathbf{Pt_3Si}$, also at $\varphi \simeq 15°$. The cuboctahedra have now collapsed to tetracapped rhombic antiprisms, and the *A* atoms have four nearest neighbours at the corners of a distorted tetrahedron.

These final examples emphasize once again the continuity between 'substitutional' and 'interstitial' alloy structure types.

This work was assisted by grants from ZWO and (to MO'K) from the US National Science Foundation.

References

AHTEE, A., AHTEE, M., GLAZER, A. M. & HEWAT, A. W. (1976). *Acta Cryst.* B**32**, 3243–3246.

ANDERSSON, S. & HYDE, B. G. (1974). *J. Solid State Chem.* **9**, 92–101.

ARONSSON, B. & NYLUND, A. (1960). *Acta Chem. Scand.* **14**, 1011–1018.

BLISTANOV, A. A., NOSOVA, I. V. & TAGIEVA, M. M. (1975). *Sov. Phys. Crystallogr.* **20**, 409–410.

BRADLEY, A. J. & TAYLOR, A. (1937). *Phil. Mag.* **23**, 1049–1067.

BRAUER, G. & ZINTL, E. (1937). *Z. Phys. Chem.* B**37**, 323–352.

BROCHU, R., PADIOU, J. & GRANDJEAN, D. (1970). *C. R. Acad. Sci. Ser. C*, **271**, 642–643.

BUERGER, M. J. & WUENSCH, B. J. (1963). *Science*, **141**, 276.

CHAO, E. C. T., EVANS, H. T., SKINNER, B. J. & MILTON, C. (1961). *Am. Mineral.* **46**, 379–393.

CHEETHAM, A. K. & NORMAN, N. (1974). *Acta Chem. Scand.* A**28**, 55–60.

CHENAVAS, J., JOUBERT, J. C., MAREZIO, M. & BOCHU, B. (1975). *J. Solid State Chem.* **14**, 25–33.

COPPENS, P. & EIBSCHÜTZ, M. (1965). *Acta Cryst.* **19**, 524–531.

DESCHIZEAUX, M. N., JOUBERT, J. C., VEGAS, A., COLLOMB, A., CHENAVAS, J. & MAREZIO, M. (1976). *J. Solid State Chem.* **19**, 45–51.

FASISKA, E. J. & JEFFREY, G. A. (1965). *Acta Cryst.* **19**, 463–471.

GELLER, S. (1956). *J. Chem. Phys.* **24**, 1236–1239.

GLAZER, A. M. (1972). *Acta Cryst.* B**28**, 3384–3392.

HEBECKER, CH. (1972). *Z. Anorg. Allg. Chem.* **393**, 223–229.

HEPWORTH, M. A., JACK, K. H., PEACOCK, R. D. & WESTLAND, G. J. (1957). *Acta Cryst.* **10**, 63–69.

HIRTHE, J. P. & LOTHE, J. (1968). *Theory of Dislocations*. New York: McGraw-Hill.

HULLIGER, F. (1968). *Struct. Bonding*, **4**, 99.

HYDE, B. G., BAGSHAW, A. N., ANDERSSON, S. & O'KEEFFE, M. (1974). *Annu. Rev. Mater. Sci.* **4**, 43–92.

HYDE, B. G., BURSILL, L. A., O'KEEFFE, M. & ANDERSSON, S. (1972). *Nature (London), Phys. Sci.* **237**, 35–38.

KARUP-MØLLER, S. & MAKOVICKY, E. (1974). *Am. Mineral.* **59**, 889–895.

KAY, H. F. & BAILEY, P. C. (1957). *Acta Cryst.* **10**, 219–226.
KJEKSHUS, A. & RAKKE, T. (1974). *Acta Chem. Scand.* A**28**, 99–103.
KOCMAN, V. & NUFFIELD, E. W. (1973). *Acta Cryst.* B**29**, 2528–2535.
KOHN, K., INOUE, K., HORIE, O. & AKIMOTO, S. (1975). *Tech. Rep. Inst. Solid State Phys., Tokyo*, Ser. A, No. 736.
LUDEKENS, W. L. W. & WELCH, A. J. E. (1952). *Acta Cryst.* **5**, 841.
MACKAY, A. L. (1962). *Acta Cryst.* **15**, 916–918.
MANSMANN, M. (1965). *Z. Kristallogr.* **122**, 375–398.
MAREZIO, M. & DERNIER, P. D. (1971). *Mater. Res. Bull.* **6**, 23–29.
MAREZIO, M., DERNIER, P. D., CHENAVAS, J. & JOUBERT, J. C. (1973). *J. Solid State Chem.* **6**, 16–20.
MAREZIO, M., REMEIKA, J. P. & DERNIER, P. D. (1970). *Acta Cryst.* B**26**, 2008–2022.
MEGAW, H. D. (1968). *Acta Cryst.* A**24**, 583–588.
MEGAW, H. D. (1973). *Crystal Structures: A Working Approach*. Philadelphia: Saunders.
MEGAW, H. D. & DARLINGTON, C. N. W. (1975). *Acta Cryst.* A**31**, 161–173.
MICHEL, C., MOREAU, J. M. & JAMES, W. J. (1971). *Acta Cryst.* B**27**, 501–503.
NOËL, H., PADIOU, J. & PRIGENT, J. (1975). *C. R. Acad. Sci. Ser. C*, **280**, 123–126.
NYBURG, S. C., OZIN, G. A. & SZYMAŃSKI, J. T. (1971). *Acta Cryst.* B**27**, 2298–2304.
NYMAN, H. (1976). *J. Solid State Chem.* **17**, 75–78.
OFTEDAL, I. (1929). *Z. Phys. Chem.* B**5**, 272–291.
OFTEDAL, I. (1931). *Z. Phys. Chem.* B**13**, 190–200.
O'KEEFFE, M. & HYDE, B. G. (1975). *J. Solid State Chem.* **13**, 172–175.
O'KEEFFE, M. & HYDE, B. G. (1976). *Acta Cryst.* B**32**, 2923–2936.
OLOFSSON, O. (1972). *Acta Chem. Scand.* **26**, 2777–2787.
RODIER, N. & LARUELLE, P. (1970). *C. R. Acad. Sci.* **270**, 2127–2130.
RUNDQVIST, S. & PRAMATUS, S. (1967). *Acta Chem. Scand.* **21**, 191–194.
SAKOWSKI-COWLEY, E. C., ŁUKASZEWICZ, K. & MEGAW, H. D. (1969). *Acta Cryst.* B**25**, 851–865.
SCHLENGER, H., JACOBS, H. & JUZA, R. (1971). *Z. Anorg. Chem.* **385**, 177–201.
SCHLYTER, K. (1952). *Ark. Kemi*, **5**, 73–82.
SCHUBERT, K. (1964). *Kristallstrukturen Zweikomponentiger Phasen*, p. 303. Berlin: Springer-Verlag.
SOBOLEV, B. P., GARASHINA, L. S., FEDOROV, P. P. & SEIRANYAN, K. B. (1974). *Sov. Phys. Crystallogr.* **18**, 473–476.
STENBERG, E. (1961). *Acta Chem. Scand.* **15**, 861–870.
WALFORD, L. K. (1964). *Acta Cryst.* **17**, 57–59.
WELLS, A. F. (1975). *Structural Inorganic Chemistry*, 4th ed., p. 124. Oxford: Clarendon Press.
WISEMAN, P. J. & DICKENS, P. G. (1973). *J. Solid State Chem.* **6**, 374–377.
ZALKIN, A. & TEMPLETON, D. H. (1953). *J. Amer. Chem. Soc.* **75**, 2453–2458.

Acta Cryst. (1977). B**33**, 3813–3816

A Simple Refinement of Density Distributions of Bonding Electrons. I. A Description of the Proposed Method

BY ERWIN HELLNER

Mineralogisches Institut and SFB 127, *Universität Marburg, Lahnberge, D*-3550 *Marburg/Lahn, Federal Republic of Germany*

(*Received* 1 *March* 1977; *accepted* 18 *June* 1977)

A partitioning of the structure factor into core electrons (c), valence (bonding) electrons (v), and non-bonding electrons (o) is proposed for a simple refinement. At the beginning of the refinement the x_i^v,y_i^v,z_i^v are located in the middle of pairs of bonded atoms of the molecule in the crystal. The charge clouds of the non-bonding electrons include lone-pair electrons, non-bonded p orbital products *etc.* At the beginning of the refinement the x_i^o,y_i^o,z_i^o are identical with the parameters of the core electrons. The distributions of the latter two charge clouds (v and o) are described by three-dimensional Gaussian functions which at the same time include the effects of thermal motion to an extent of about 10% of the B_{ij} parameters. A separation of the thermal and charge distribution is intended. A comparison of different methods for least-squares refinements with this simple method is made.

Introduction

Grimm, Brill, Hermann & Peters (1938) published electron density maps of NaCl, Mg and diamond with the F's as coefficients of a Fourier series. In the meantime efforts have been made to include the aspherical part of the charge density, which can be seen in $F_X - F_N$ maps, in a least-squares refinement. Separate